Combination of AFM, SKPFM, and SIMS to Study the Corrosion Behavior of S-phase particles in AA2024-T351

Loïc Lacroix,[a,*] Laurence Ressier,[b] Christine Blanc,[a,,z] and Georges Mankowski[a]**

[a]*Centre Interuniversitaire de Recherche et d'Ingénierie des Matériaux, Unité Mixte de Recherche CNRS 5085,*
Ecole Nationale Supérieure des Ingénieurs en Arts Chimiques et Technologiques,
31077 Toulouse Cedex 04, France
[b]*Laboratoire de Physique et Chimie des Nano-Objets (LPCNO), Unité Mixte de Recherche CNRS 5215,*
Institut National des Sciences Appliquées, 31077 Toulouse Cedex 04, France

The dissolution mechanism of S-phase particles in 2024-T351 aluminum alloy at open-circuit potential in chloride-containing sulfate solutions was investigated using atomic force microscopy (AFM), scanning Kelvin probe force microscopy (SKPFM), and secondary ion mass spectroscopy (SIMS). The combination of the three techniques allowed the correlation between SKPFM measurements and the corrosion behavior of AA2024 to be confirmed, leading to a better understanding of the electrochemical behavior of S-phase particles. A three-step mechanism for the dissolution and accompanying processes occurring near S particles was proposed: (*i*) preferential aluminum and magnesium dissolution, (*ii*) galvanic coupling between the copper-enriched particles and the surrounding matrix, leading to an increased passivity of the matrix around the particles, and (*iii*) copper deposition around the corroded particles.

[DOI: 10.1149/1.2833315]

2024 aluminum alloy is often used in aerospace applications. It is a high-strength alloy in which a heterogeneous microstructure is obtained by thermomechanical processing to obtain optimal mechanical properties. During solidification of the alloy, two kinds of coarse insoluble intermetallic particles (IPs) are formed: S-phase particles (Al_2CuMg particles) and particles containing Al, Cu, Mn, and Fe as main elements. The importance of such particles as initiation sites for localized corrosion in many electrolytes and their electrochemical behavior have been discussed in several papers.[1-10] During immersion at open-circuit potential in chloride-containing solutions, S-phase particles undergo preferential dissolution of Al and Mg, which leads to copper enrichment of the particles. Copper redistribution has been studied in various papers and was found to be related to both particle dissolution and matrix dealloying.[3,11] Secondary ion mass spectroscopy (SIMS) was found to be a powerful tool to study copper redeposition after dissolution of the copper-rich particles at low potentials in chloride-containing nitrate solutions.[12] However, some questions remain regarding the dissolution mechanism of S-phase particles. In particular, classical electrochemical methods lack lateral resolution and give no direct information about chemical-composition variations.

The corrosion behavior of the S-phase particles (IPs for simplicity in the present text) was studied in a previous paper by coupling atomic force microscopy (AFM), scanning Kelvin probe force microscopy (SKPFM), and energy-dispersive spectroscopy on more than 300 particles.[13] Before corrosion, the chemical composition of the S-phase particles was found to be highly reproducible (atom %: Al 52.6 ± 0.5, Cu 22.1 ± 0.2, Mg 25.1 ± 0.3), and their mean SKPFM potential difference with the matrix was about −90 ± 45 mV; in the as-polished sample, S-phase particles were thus found to be nobler than the matrix. After 1 h of immersion in a 0.1 M Na_2SO_4 solution with 0.001 M NaCl at room temperature, a highly heterogeneous dissolution from one IP to another (from tens to several hundreds of nanometers dissolution depth), and even heterogeneities around one particle, was demonstrated; this could be related to oxide film defects. Corroded IPs were characterized by a mean SKPFM potential, compared to the matrix, of −410 ± 110 mV. No potential difference was observed between the uncorroded IPs and the matrix. A local study was thus performed by measuring the dissolution depth, the SKPFM potential difference with the matrix (denoted by the authors[13] simply as the SKPFM potential), and the chemical composition at a given point on numerous S-phase particles. The results revealed that the IP dissolution parallels an increase of the SKPFM potential difference between the matrix and the particles and a copper enrichment of the particles (the copper content of the corroded S-phase particles can reach more than 60 atom %). This study also pointed out the necessity for a statistical analysis over a large number of S-phase particles to draw relevant quantitative conclusions about their dissolution behavior. In such conditions, SKPFM was thus found to be a powerful tool for the investigation of localized corrosion in AA2024.

But, SKPFM measurements and analyses have to be carried out with many precautions. At first, some limitations inherent to the technique have to be taken into account.[14] In particular, measurements performed on highly pitted and roughened surfaces, obtained after corrosion tests, can provoke a cross-talk of the topography and hence can give erroneous potential contrast. Furthermore, the correlation between galvanic activity and potential measured by SKPFM in air is often postulated but rarely really demonstrated. Rohwerder et al.[15] showed in a recent paper that such a correlation is not of general validity and that systematical studies must be performed for each alloy. For an alloy, a statistical study about the correlation between the SKPFM potential and the corrosion potential can make this correlation relevant.

In this paper, this correlation is investigated by combining, for the first time to our knowledge in the literature, SKPFM experiments and high-resolution chemical analyses by SIMS. The study was performed on the same zones of various S-phase intermetallics of AA2024 before and after immersion in chloride-containing sulfate medium to correlate the SKPFM potential with the local chemical composition (for S-phase particles and the oxide layers on their surface and on the surrounding matrix).

Experimental

Material and samples.— An AA2024-T351 rolled plate (wt %: Cu 4.50, Mg 1.44, Mn 0.60, Si 0.06, Fe 0.13, Zn 0.02, and Ti 0.03) with a thickness of 50 mm was used for the study. The T351 temper corresponds to a solution heat-treatment at 495°C (+/−5°C), water quenching, straining, then tempering at room temperature for 4 days.

The samples were 4 × 2 × 2 mm parallelepipeds, embedded in epoxy resin with an 8 mm^2 area exposed to the electrolyte. Special

* Electrochemical Society Student Member.
** Electrochemical Society Active Member.
z E-mail: Christine.Blanc@ensiacet.fr

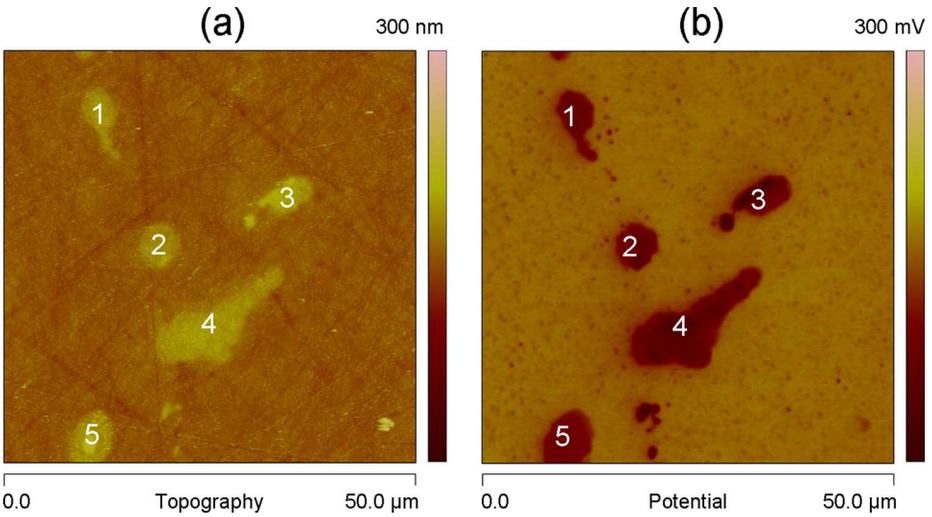

Figure 1. (Color online) (a) AFM and (b) SKPFM observations of an AA2024 sample in the as-polished state. In the SKPFM map (b), the five S-phase particles, 1–5, appear in dark contrast and thus appear nobler than the matrix.

care was taken for sample preparation, which is crucial for obtaining reliable results.[16] The samples were mechanically polished with up to 4000 grit SiC paper, then with 3 μm diamond paste, down to $\frac{1}{4}$ μm diamond paste using ethanol as lubricant. They were finally ultrasonically cleaned in ethanol and air-dried.

Corrosion tests.— Corrosion tests consisted of immersion at the open-circuit potential in a 0.1 M Na_2SO_4 solution with 0.001 M NaCl at room temperature. All chemicals used were analytical reagent grade.

Special care was taken for corroded samples; before any drying, the samples were ultrasonically cleaned in water to dissolve the corrosion products and to avoid any precipitation of sulfate and chloride crystals from the drying solution. The samples were finally ultrasonically cleaned in ethanol and air-dried to limit any effect of the adsorbed layer on the SKPFM potentials.

AFM and SKPFM measurements.— AFM and SKPFM measurements were performed on a Nanoscope IIIa Multimode atomic force microscope from Digital Instruments, in air at room temperature and an ambient relative humidity of about 40%. SKPFM mapping was carried out with a lift height of 50 nm, which was found to be the optimal value to limit cross-talk with topography and to obtain a lateral resolution of less than 100 nm. The technique and procedure used are detailed in a previous paper.[13]

Contrary to other authors who invert the SKPFM potential data in order to obtain the same polarity as the electrochemical potentials,[2,14,17] all the potential maps presented here used raw data. Thus, in this convention, dark contrasts correspond to phases nobler than the matrix. Because we often checked that the tip used was stable in potential and were only interested in potential differences between the S-phase particles and the matrix, we did not need to calibrate the potential measurements by comparison to the potential measured on pure Ni or Pt.[2,14,18] By assuming that, far from the particles, there is no significant variation of the matrix potential, we defined the potential of an S-phase particle by the difference of the SKPFM potential between the S-phase particle and the matrix remote from the particle. As previously said, the potential of S-phase particles is thus denoted in the following as SKPFM potential.

For each sample, SKPFM measurements were carried out before and after immersion on several areas containing only S-phase particles. On highly corroded S-phase particles, scan rates as low as 0.1 Hz were sometimes required to accurately map the topography by AFM, which is a crucial prerequisite to get nonerroneous SKPFM measurements.[14]

SIMS analysis.— The local chemical composition of the S-phase intermetallics and of the oxide layer grown on and around the IPs was analyzed by SIMS using an IMS 4F/6F CAMECA analyzer. Six signals were collected during the analysis: ^{23}Na, ^{24}Mg, ^{27}Al, ^{55}Mn, ^{56}Fe, and ^{63}Cu. High-resolution mode was used to avoid interference between the different signals.

Analyses were performed on the same areas after different sputtering times to study the variation of the chemical composition on the sample surface due to immersion in the electrolyte.

Results and Discussion

Formation of an oxide layer on the uncorroded S particles.— Figure 1 shows typical AFM topographic (Fig. 1a) and SKPFM (Fig. 1b) observations of an AA2024 sample in the as-polished state. On the AFM topographic map, five Al_2CuMg particles (numbered 1–5) can be distinguished due to their rounded shape. They protrude slightly from the surface (between +30 and +90 nm) because of their greater hardness and lower polishing rate relative to the matrix. The SKPFM map (Fig. 1b), on the same area of the as-polished sample, reveals that the S-phase particles have a lower potential than the matrix, and they are thus nobler than the matrix. Finally, the high lateral resolution of SKPFM allows intermetallics as small as 400 nm to be resolved.

Figure 2 presents AFM topographic (Fig. 2a), SKPFM (Fig. 2b), and SIMS (Fig. 2c) observations of the same zone after 90 min immersion in a 0.1 M Na_2SO_4 + 0.001 M NaCl solution. Figure 2a reveals that IPs 1, 2, 3, and 5 remained unattacked because they kept on protruding slightly, while IP 4 was corroded to a dissolution depth of 500 nm. This confirms that the corrosion initiation or/and propagation are highly heterogeneous and that a statistical approach is necessary to obtain relevant quantitative results about the dissolution kinetics.[13] The potential map (Fig. 2b) shows that IP 4, which dissolved, presents an increased potential difference with the matrix (from −120 to −420 mV) in comparison with the as-polished state (Fig. 1b). It is known that S-phase particle dissolution causes copper enrichment, leading to ennoblement of the particle. As copper is nobler than aluminum and magnesium, this chemical evolution corresponds to a greater SKPFM potential difference with the matrix. As explained in the experimental part, in the convention used by the authors, the lower the SKPFM potential, the nobler the particle with respect to the matrix. Dissolution can thus be followed by AFM and SKPFM, with the potential values of the particles decreasing. As seen in Fig. 2b, uncorroded particles (IPs 1, 2, 3, and 5) are no longer visible on the SKPFM potential map after 90 min of immersion. This is in perfect agreement with the chemical composition seen on the SIMS maps (Fig. 2c), where neither Cu nor Mg can be detected on the top of the unattacked particles. These observations suggest that a thick oxide layer covers the unattacked zones.

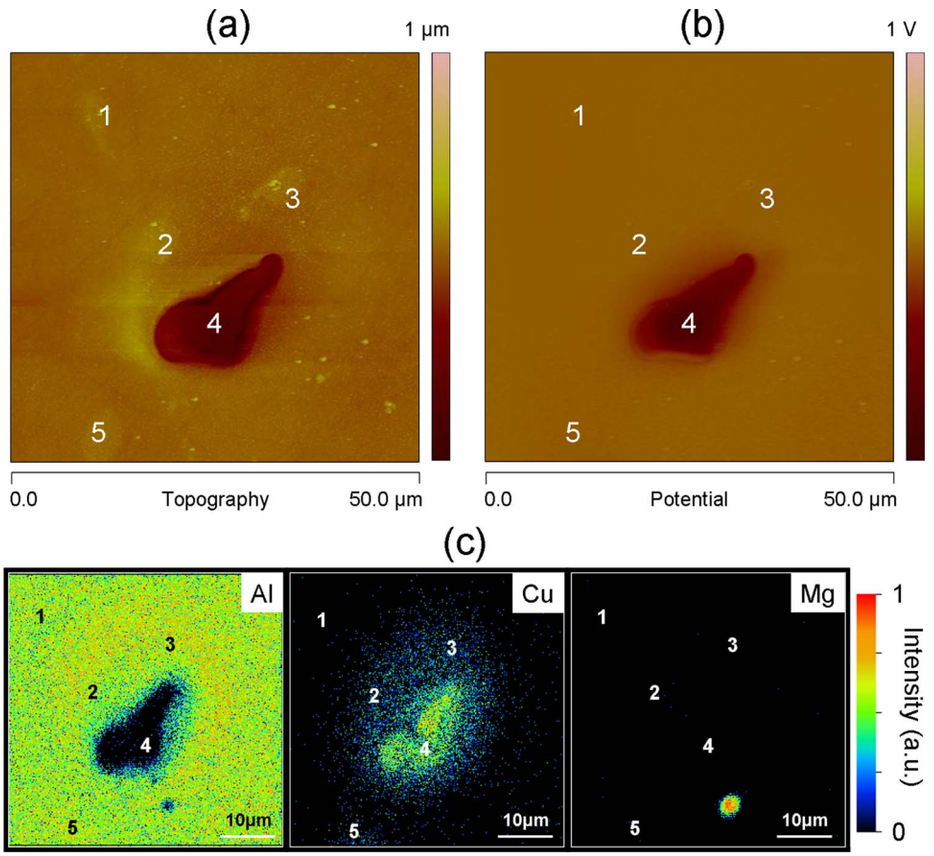

Figure 2. (Color online) (a) AFM, (b) SKPFM, and (c) SIMS observations of the same zone as in Fig. 1 after immersion for 90 min in a 0.1 M Na_2SO_4 + 0.001 M NaCl solution.

In order to confirm the hypothesis of a covering oxide layer, sputtering was carried out by SIMS on the same area to remove approximately 300 nm off the top. Figure 3 shows AFM topographic (Fig. 3a), SKPFM (Fig. 3b), and SIMS observations (Fig. 3c) of the area refreshed after sputtering. The AFM topographical map does not differ much from that recorded before sputtering (Fig. 2a) (except a dust particle present on the corroded particle IP 4); unattacked particles still protrude, and the corroded particle is still well below the surface. However, a dust particle can be seen to have settled on IP 4. Unlike in previous SKPFM and SIMS analyses (Fig. 2), unattacked particles can now be distinguished after sputtering on the potential (Fig. 3b) and SIMS maps (Fig. 3c). Unattacked particles are seen on the SIMS maps as a lack of Al and an excess of Cu and Mg in comparison with the matrix, which is in agreement with their chemical composition before immersion. The corroded particle (IP 4) is characterized by a lack of Al and an excess of Cu in comparison with the unattacked particles. The absence of a Mg signal is in agreement with the dissolution mechanism of S-phase particles.[19]

These results thus confirm that the S-phase intermetallics can present different corrosion behavior when immersed in the chloride-containing sulfate electrolyte; some particles do not dissolve and an oxide layer forms on their surface, while other particles corrode with Al and Mg dissolution. The combination of SIMS and SKPFM techniques proves that SKPFM is really sensitive to the extreme surface chemical composition and allows the dissolution mechanism of Cu-rich particles to be followed. When a particle does not dissolve and becomes covered by an oxide layer, no SKPFM potential difference with the matrix is observed, while the dissolution mechanism with copper enrichment leads to a greater SKPFM potential difference with the matrix.

Formation of a copper deposit around the corroded S particles.— Comparison of Fig. 1b and 2b also reveals a slight broadening of the potential of the corroded S-phase particle (IP 4) after immersion. This broadening is observed for all corroded particles. It appears more clearly in another area of the same sample by comparing Fig. 4b and 5b. Figure 4 shows AFM topographic (Fig. 4a) and SKPFM (Fig. 4b) observations of an AA2024 as-polished sample and reveals five S-phase particles (numbered 1′ to 5′). As previously observed, the IPs appear with a SKPFM potential lower than that of the matrix. The same zone was observed after 90 min of immersion in a 0.1 M Na_2SO_4 + 0.001 M NaCl solution (Fig. 5). The AFM topographic picture (Fig. 5a) reveals that IPs 1′, 2′, and 4′ corroded, while IPs 3′ and 5′ remained unattacked. In agreement with previous observations, in the SKPFM map there is no potential difference between the uncorroded IPs and the matrix (Fig. 5b) because of the oxide layer recovering them. The corroded particles appear with a potential difference with respect to the matrix much greater than in the as-polished state (Fig. 4b), which is attributed to the copper enrichment of the particles. Furthermore, unlike observations before immersion (Fig. 4) where the SKPFM maps fit the topographical maps exactly, corroded IPs are characterized by a broadened potential which overlaps the contour of the particles (dotted line in Fig. 5b). SIMS experiments performed on the same zone revealed that the potential broadening can be attributed to the copper deposit (Fig. 5c), as often reported in the literature.[3,11,19]

To confirm this assertion, a thin layer of the surface was removed by SIMS sputtering and corresponds to the removal of about 30 nm of material. Figure 6 presents AFM topographic (Fig. 6a), SKPFM (Fig. 6b), and SIMS observations (Fig. 6c) of this refreshed area after sputtering. No potential broadening is observed any longer on the SKPFM map, and SIMS measurements confirm that the copper deposit no longer exists because copper is now only detected on a zone strictly limited to the particle area (Fig. 6c). Figure 7 shows potential sections of particle 2′ (marked as a dashed line on the potential maps of Fig. 4b, 5b, and 6b), plotted, respectively, for the as-polished sample (solid line in Fig. 7), after 90 min immersion in

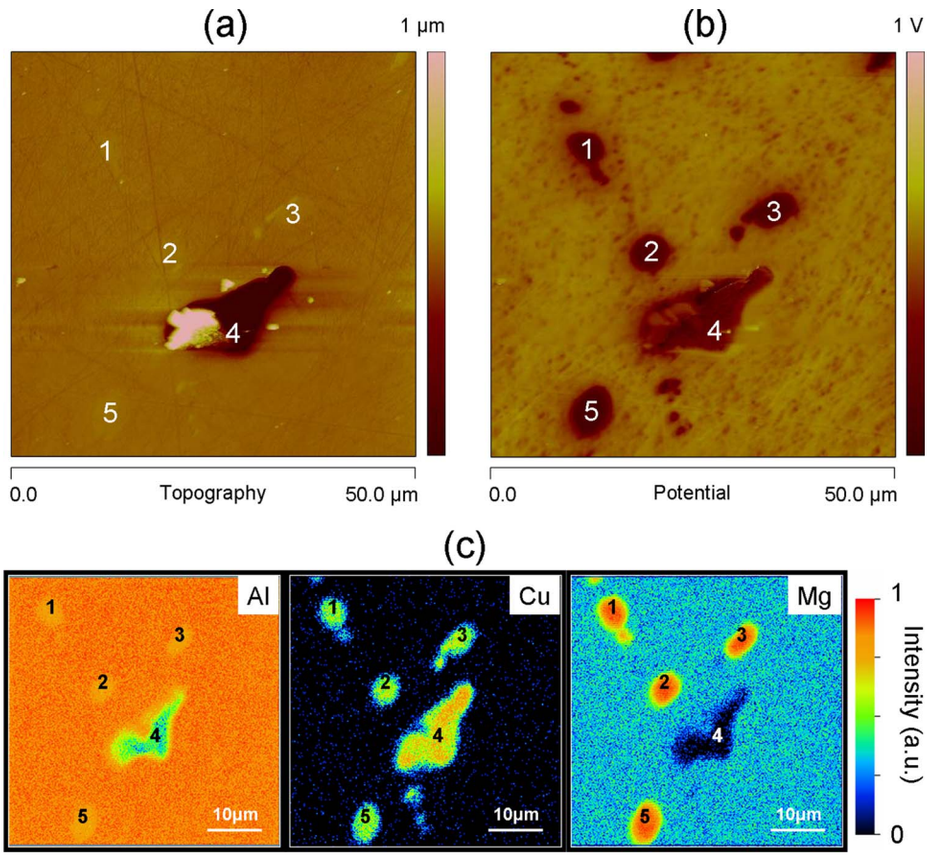

Figure 3. (Color online) (a) AFM, (b) SKPFM, and (c) SIMS observations of the same zone as in Fig. 2 after SIMS sputtering, which removed about 300 nm of material.

a 0.1 M Na_2SO_4 + 0.001 M NaCl solution (dotted line in Fig. 7), and after SIMS sputtering (dashed line in Fig. 7). This graph reveals that the copper deposit is about 2.5 times larger in diameter than the corroded particle. The results thus show that SKPFM is sensitive enough to detect the formation of a copper deposit (less than 30 nm thick) around the intermetallics. The potential map is not as homogeneous as that of the first zone studied after sputtering (Fig. 3b). In fact, the sputtering just removed a thin layer of about 30 nm, which did not allow the entire oxide layer grown during immersion to be removed. Some heterogeneities coming from the remnant oxide layer can thus be seen on the SKPFM map.

Galvanic coupling between S-phase particles and the surrounding matrix.— Additional results can be obtained by analyzing more accurately the Al and Mg signals measured by SIMS. In Fig. 5, an approximately 6 µm wide ring around the particles, about 5 µm away from them, can be observed both in the AFM topographic picture and the Al SIMS map (dashed ring). It corresponds to a stronger intensity of Al signal in the SIMS map. This can be related to an alumina layer that is slightly thicker in this zone, because the oxidized state of aluminum has a higher emission rate. This shows the increased passivity of the aluminum matrix surrounding the particles except at the matrix/particle interface. The result is in good

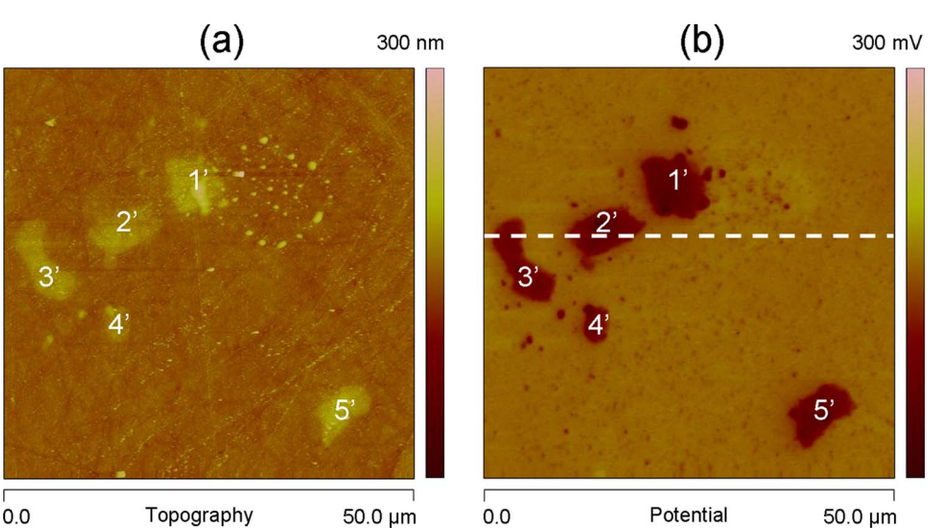

Figure 4. (Color online) (a) AFM and (b) SKPFM observations of another zone of an AA2024 sample in the as-polished state. In the SKPFM map (b), the five S-phase particles, 1′–5′, appear in dark contrast and thus appear nobler than the matrix.

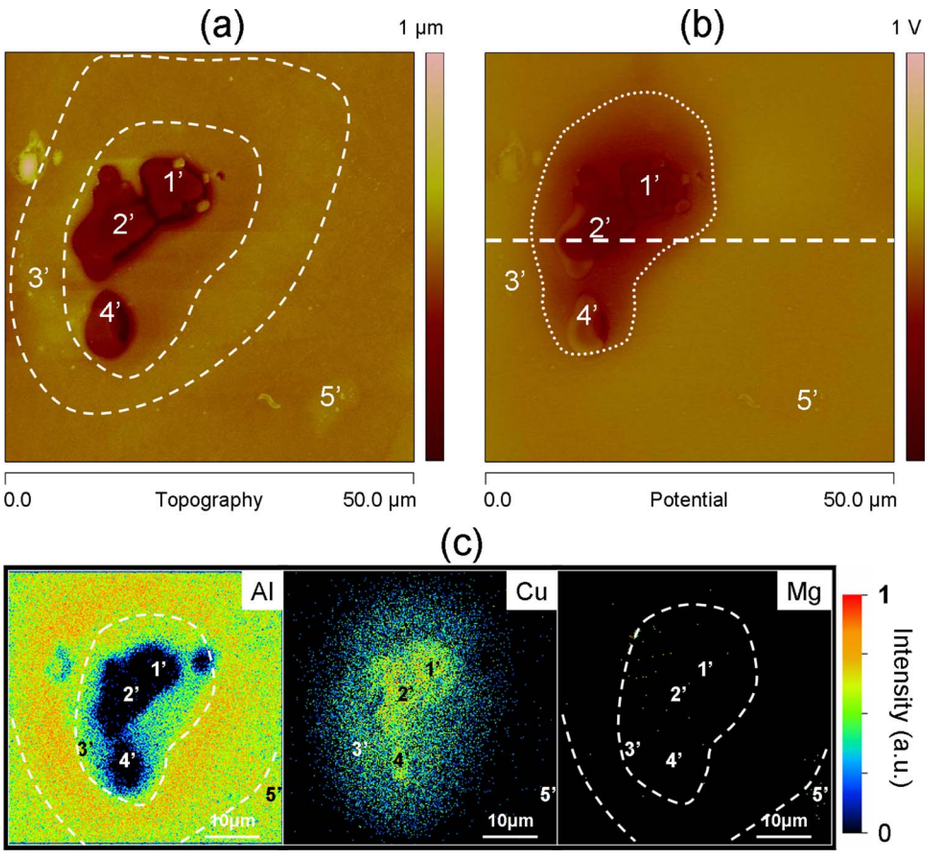

Figure 5. (Color online) (a) AFM, (b) SKPFM, and (c) SIMS observations of the same zone as in Fig. 4 after immersion for 90 min in a 0.1 M Na_2SO_4 + 0.001 M NaCl solution.

agreement with previously published results.[20] Jorcin et al. demonstrated that coupling between pure aluminum and pure copper leads to an increased passivity of the aluminum except at the aluminum/copper interface. In this paper, the surrounding Al matrix (except at the aluminum/copper interface) acts as a local anode and hence shows greater passivity, while the copper deposit and the copper-enriched particles act as a local cathode. This galvanic coupling mechanism can be confirmed by analyzing the Mg signal in Fig. 6c. The SIMS sputtering allowed the copper deposit to be removed, and thus the magnesium signal from the matrix can be detected close to the particles (Fig. 6c), while it was invisible before sputtering (Fig. 5c). Furthermore, far from the corroded particles, IP 1′, 2′, and 4′ (just after the dashed ring, Fig. 6c), the SIMS sputtering allowed the Mg signal of both the matrix and IP 5′ to be detected also, because the alumina layer was removed. For the same reasons, IP 5′ is now visible on the SKPFM map, Fig. 6b. However, on the aluminum matrix part with increased passivity (dashed rings in Fig. 5c and 6c), the alumina layer was so thick that the Mg signal from the matrix could not be detected even after sputtering (Fig. 6c). The matrix was probably still covered in this part by the remnant alumina layer after sputtering.

Mechanism for dissolution and accompanying processes occurring near the S particles.— Several papers have reported descriptions of the S-phase dissolution mechanism in AA2024.[1,3,11] A dissolution/back-plating copper redistribution mechanism during corrosion of AA2024-T3 alloy is commonly assumed. Buchheit et al. proposed a complex mechanism based on S-phase dealloying leading to mechanically detached Cu clusters, followed by oxidation and back-plating on the surrounding matrix.[3] Vukmirovic et al. postulated that the copper redistribution is half supported by both the dissolution/back-plating mechanism of S-phase and adjacent matrix dealloying.[11] In a previous work, the nanoporous morphology of corroded particles was reported.[13]

From results found in the literature and the present study, a mechanism for the dissolution and accompanying processes occurring near copper-rich particles at open-circuit potential can be proposed. Figure 8 schematically illustrates it; an S-phase particle is represented in an aluminum matrix immersed in a chloride-containing sulfate solution. During immersion, the particle undergoes selective dissolution with a first step involving preferential release of Al and Mg (Fig. 8a), which leads to copper enrichment and a porous structure of the particle (Fig. 8b). This chemical evolution of the particle enhances its cathodic behavior, so oxygen reduction takes place at its surface (Fig. 8b). The galvanic coupling between the particle (cathodic site) and the surrounding matrix (anodic site) explains the increased passivity behavior of the adjacent matrix zone except at the matrix/particle interface (Fig. 8b). Indeed, at the interface, increased oxygen reduction takes place, leading to local alkalinization, which causes the destabilization of the alumina layer on the matrix and the formation of a deep trench on the aluminum matrix all around the particle.[3,20] Due to the porous structure of the corroded particle,[13] copper clusters can become detached from the intermetallic and form a deposit around it. Then, there is galvanic coupling between both the copper-enriched particle and the copper deposit with the surrounding matrix, which can enhance the passivity of the surrounding matrix even further. In this zone, the alumina layer can be thick enough to preserve some S-phase particles from corrosion (this is the case of particle 3′ in Fig. 5). In contrast, the dissolution of the matrix at the matrix/particle interface continues so that S-phase particles can become detached (Fig. 8c).

Conclusions

AFM, SKPFM, and SIMS experiments were successfully performed on AA2024 to study the corrosion behavior of S-phase particles at open-circuit potential in chloride-containing sulfate solutions. The combination of the three techniques allowed the

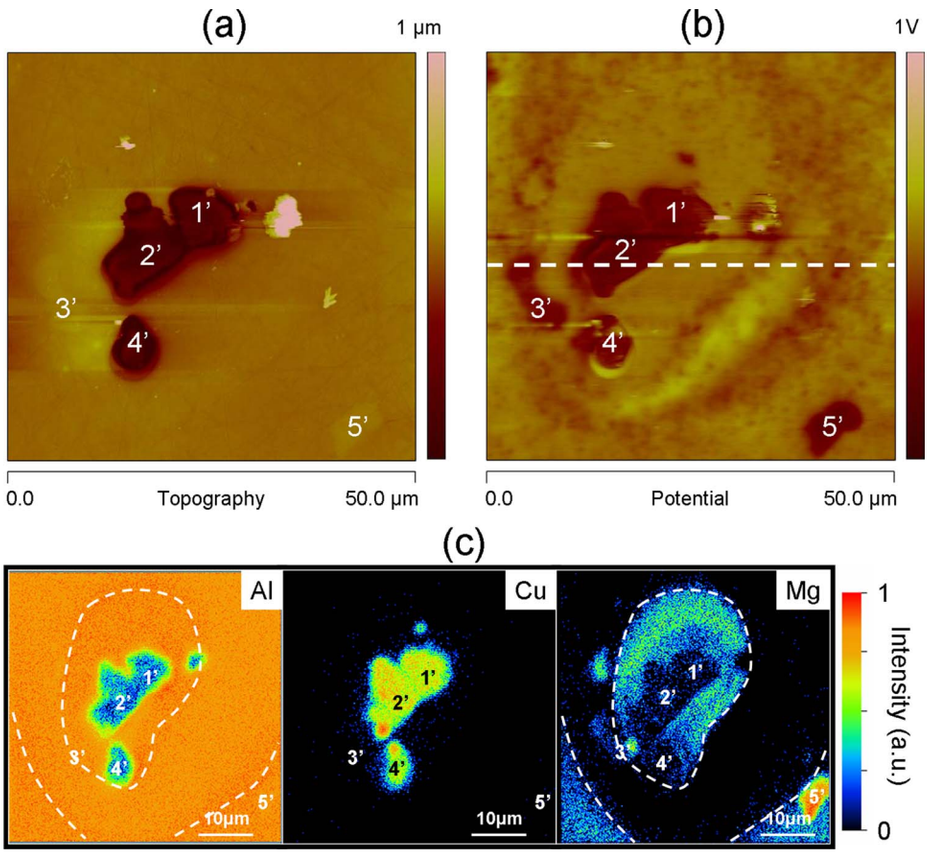

Figure 6. (Color online) (a) AFM, (b) SKPFM, and (c) SIMS observations of the same zone as in Fig. 5 after SIMS sputtering, which removed about 30 nm.

correlation between SKPFM measurements and the corrosion behavior of AA2024 to be proven, leading to a better understanding of the electrochemical behavior of S-phase particles. The following conclusions can be made.

1. SKPFM is an efficient technique to study the corrosion behavior of S-phase particles in AA2024. On immersion in the electrolyte, the absence of SKPFM potential contrast on uncorroded S-phase particles could be caused by some S-phase particles being covered by an alumina film, protecting them from subsequent dissolution. Moreover, the broadening of SKPFM potentials on corroded S-phase particles is due to the deposition of copper around them.

2. A three-step mechanism for the dissolution and accompanying processes occurring near the AA2024 S-phase particles at open circuit in chloride-containing sulfate solutions can be proposed: (*i*) Al and Mg preferential dissolution, (*ii*) galvanic coupling between the Cu-enriched particles and the surrounding matrix, leading to increased passivity of the surrounding matrix, and (*iii*) Cu deposition around the corroded particles.

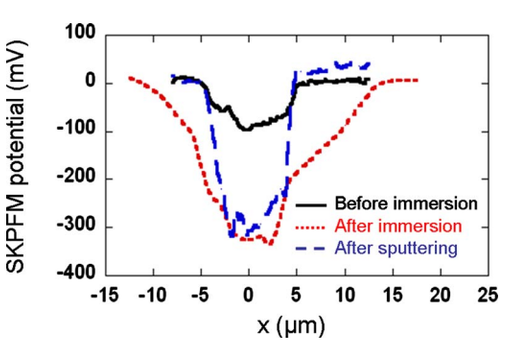

Figure 7. (Color online) SKPFM sections of the particle marked 2′ in Fig. 4b, 5b, and 6b before immersion (solid line), after immersion for 90 min in a 0.1 M Na_2SO_4 + 0.001 M NaCl solution (dotted line), and after SIMS sputtering (dashed line).

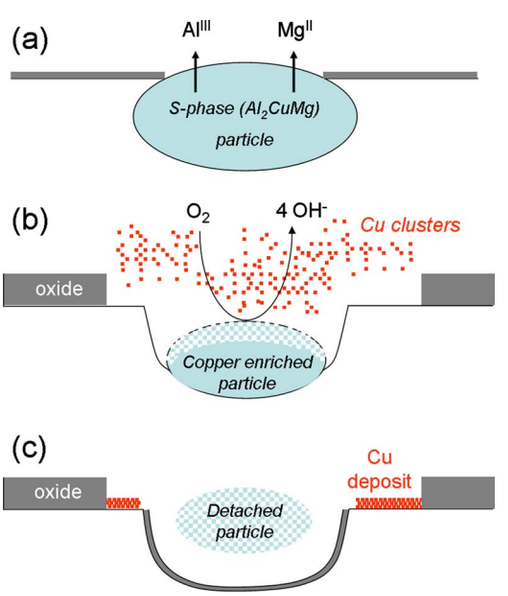

Figure 8. (Color online) Schema (not to scale) of the mechanism for the dissolution and accompanying processes occurring near an S-phase particle at open-circuit potential in a chloride-containing sulfate solution.

Acknowledgments

The authors thank Claude Armand from the Institut National des Sciences Appliquées de Toulouse for the SIMS analysis.

Centre National de Recherche Scientifique assisted in meeting the publication costs of this article.

References

1. C. Blanc, B. Lavelle, and G. Mankowski, *Corros. Sci.*, **39**, 495 (1997).
2. P. Schmutz and G. S. Frankel, *J. Electrochem. Soc.*, **145**, 2285 (1998).
3. R. G. Buchheit, M. A. Martinez, and L. P. Montes, *J. Electrochem. Soc.*, **147**, 119 (2000).
4. Z. Szklarska-Smialowska, *Corros. Sci.*, **41**, 1743 (1999).
5. J. W. J. Silva, A. G. Bustamante, E. N. Codaro, R. Z. Nakazato, and L. R. O. Hein, *Appl. Surf. Sci.*, **236**, 356 (2004).
6. A. Garner and D. Tromans, *Corrosion (Houston)*, **35**, 55 (1979).
7. X. Zhao, G. S. Frankel, B. Zoofan, and S. Rokhlin, *Corrosion (Houston)*, **59**, 1012 (2003).
8. M. Posada, L. E. Murr, C. S. Niou, D. Roberson, D. Little, R. Arrowood, and D. George, *Mater. Charact.*, **38**, 259 (1997).
9. M. R. Bayoumi, *Eng. Fract. Mech.*, **54**, 879 (1996).
10. X. Liu, G. S. Frankel, B. Zoofan, and S. Rokhlin, *Corros. Sci.*, **49**, 139 (2007).
11. M. B. Vukmirovic, N. Dimitrov, and K. Sieradzki, *J. Electrochem. Soc.*, **149**, B428 (2002).
12. C. Blanc, S. Gastaud, and G. Mankowski, *J. Electrochem. Soc.*, **150**, B396 (2003).
13. L. Lacroix, L. Ressier, C. Blanc, and G. Mankowski, *J. Electrochem. Soc.*, **155**, C8 (2008).
14. T. H. Muster and A. E. Hughes, *J. Electrochem. Soc.*, **153**, B474 (2006).
15. M. Rohwerder and F. Turcu, *Electrochim. Acta*, **53**, 290 (2007).
16. B. S. Tanem, G. Svenningsen, and J. Mardalen, *Corros. Sci.*, **47**, 1506 (2005).
17. J. H. W. de Wit, *Electrochim. Acta*, **49**, 2841 (2004).
18. P. Schmutz and G. S. Frankel, *J. Electrochem. Soc.*, **145**, 2295 (1998).
19. C. Blanc and G. Mankowski, *Corros. Sci.*, **40**, 411 (1998).
20. J.-B. Jorcin, C. Blanc, N. Pébère, B. Tribollet, and V. Vivier, *J. Electrochem. Soc.*, **155**, C46 (2008).